

Supplementary Information

Diversity at the nanoscale: Laser-oxidation of single-layer graphene affects Fmoc-phenylalanine surface-mediated self-assembly

Johanna Schirmer,^a Romain Chevigny,^a Aleksei Emelianov,^a Eero Hulkko,^{a,b} Andreas Johansson,^{a,c} Pasi Myllyperkiö,^a Efstratios D. Sitsanidis, *^a Maija Nissinen *^a and Mika Pettersson *^a

^a*Department of Chemistry, Nanoscience Center, University of Jyväskylä, P. O. Box 35, FI-40014 JYU, Finland. E-Mail: mika.j.pettersson@jyu.fi, efstratios.d.sitsanidis@jyu.fi*

^b*Department of Biological and Environmental Sciences, Nanoscience Center, University of Jyväskylä, P. O. Box 35, FI-40014 JYU, Finland.*

^c*Department of Physics, Nanoscience Center, University of Jyväskylä, P. O. Box 35, FI-40014 JYU, Finland.*

Table of Contents

S1. Experimental and computational details	2
S2. Sample optimization	5
S3. Characterization of concentric crystals.....	7
S4. Raman spectroscopy of pristine and oxidized graphene	8
S5. Nano-FTIR spectra locations and description	9
S6. Density Functional Theory calculations	10
S7. References	15

S1. Experimental and computational details

Materials

Fluorenylmethoxycarbonyl-Phenylalanine, Fmoc-Phe, was purchased from TCI (Japan). Phosphate Buffer Saline tablets (PBS, NaCl 137 mM, phosphate buffer 10mM, KCl 2.7 mM, pH 7.4) were purchased from Fisher Scientific (United Kingdom) and used as described by the manufacturer.

Sample Preparation

Single layer graphene (SLG) surface preparation. Graphene was synthesized on Cu (111) thin films evaporated onto single-crystal sapphire (0001) substrates. The catalyst film was annealed at 1060 °C under the gas flows of argon (470 sccm) and hydrogen (27 sccm) for 30 min to promote mono-crystallinity through secondary grain growth. After annealing, graphene growth was initiated by adding 6.8 sccm of 1% methane in argon to the furnace while keeping the temperature at 1060 °C. The growth time was 25 min. The graphene films were transferred by a standard PMMA transfer method onto a silicon substrate (5 mm x 5 mm) with a 300 nm thermal oxide film and a palladium reference grid on top. The PMMA film was removed with acetone (30 min at 50 °C). Finally, the sample was annealed at 300 °C in Ar/H₂ atmosphere for two hours to remove PMMA residues.

Laser-Oxidation. Two-photon oxidation of graphene was performed with a 515 nm femtosecond laser (Pharos-10, Light Conversion Ltd., 600 kHz repetition rate, 250 fs pulse duration, Lithuania) in an ambient atmosphere with a relative humidity of 35%. To pattern ten 40 x 400 μm² areas, 4x objective was used with a spot diameter of approximately 6 μm. The pulse energy was set to 3 nJ, and the time of irradiation was 0.1 s/spot with a 2 μm step separation. Laser-oxidation of graphene was confirmed by Raman spectroscopy (section S4).

Gel sample preparation. Fmoc-Phe (1 mg, 2 mg or 3 mg) and PBS (1 mL, 0.1 M, pH = 7.4) were mixed and sonicated to obtain a fine suspension. Subsequently, the suspension was heated at 80 °C for 30 min to a transparent, colourless solution. 2 μL of the hot Fmoc-Phe solution were added on top of the SLG surface. The solution was let to cool down overnight at room temperature in a water-saturated environment. The remaining Fmoc-Phe solution was kept in a closed vial overnight to ensure gelation had occurred. Three different types of samples were produced, namely room temperature (rt) samples, rt-vacuumed samples, and lyophilized samples.

Next day, rt samples were transferred to a half-open petri dish and left to dry overnight at rt. The rt-vacuumed sample was transferred into a glass vial and dried under vacuum ($p < 1$ mbar) at rt. The lyophilized samples were transferred to glass vials and stored overnight at -20 °C. Next day, the lyophilized samples were dried for 30 min at -50 °C under vacuum ($p < 1$ mbar). The list of samples with the respective Fmoc-Phe concentration c and the drying method are listed in table S1.

Table S1: List of prepared samples type of surface, Fmoc-Phe concentration and drying method.

Substrate	$c_{\text{Fmoc-Phe}}$ (w%)	Drying method
Mica	0.1	rt
Mica	0.2	rt
Mica	0.3	rt
Mica	0.1	rt-Vacuum
Mica	0.1	Lyophilization
prG	0.1	rt
prG/oxG	0.1	Lyophilization

Sample Characterization

Optical microscopy. Optical images were taken with an Olympus microscope, equipped with 5x, 10x, 20x and 50x objectives and a camera. All images were processed with Fiji2 software.

Atomic force microscopy (AFM). AFM imaging was performed in air on a Bruker Dimension Icon AFM, operated in PeakForce Tapping mode. Scan-Asyst-AIR probes (Bruker, USA) made from silicon nitride with a spring constant of 0.4 N/m were employed, and the PeakForce Setpoint was 2 nN for all images.

The obtained data was processed and analysed with Nanoscope Analysis 1.9 software. The roughness of pristine and laser-oxidized graphene was calculated with the roughness analysis function, and fibre height and width were measured with the section analysis function. AFM images for figures were created with the Gwyddion software. The significance of the difference in fibre height was determined in OriginPro 2017 software with a One-way ANOVA test ($p < 0.001$).

Scattering-type scanning near-field optical microscopy (s-SNOM). The s-SNOM experiments were performed on a neaSNOM device (attocube systems AG, Germany) equipped with a tuneable quantum cascade laser for s-SNOM imaging and a broadband laser continuum for nano-FTIR spectroscopy.

For imaging experiments, Arrow-NCpt-50 silicon probes (Nanoworld® AG, Switzerland) with a Pt/Ir coating on the tip and detector side and a resonance frequency of 285 kHz were used. Six images were taken in the same location with different MIR frequencies (1546 cm⁻¹, 1600 cm⁻¹, 1645 cm⁻¹, 1672 cm⁻¹, 1699 cm⁻¹, 1720 cm⁻¹) on a pristine graphene surface. The images were taken with a resolution of 10 nm and processed with the Gwyddion software. A plane fit was applied to remove the thermal drift of the microscope. Due to a maladjustment of the mirror amplitude, the images at 1699 cm⁻¹ and 1645 cm⁻¹ showed an inverse optical phase contrast. The phase values were corrected for analysis by inversion. For the analysis of the absorptive properties at specific locations, the phase values of five pixels in the respective location were averaged.

Metal-coated nanospectroscopy probes were used for nano-FTIR experiments. Initially, an AFM topographic image was taken from the area of interest. Subsequently, nano-FTIR spectra were taken from the desired spots, including background spectra from outside the region covered with gel (pristine and oxidized graphene). The used frequency range was 1500 cm⁻¹ to 1800 cm⁻¹. The integration time per pixel was 80 ms and the spectral resolution ≈15 cm⁻¹. Each spectrum was divided by the corresponding background spectrum. The phase offset was manually adjusted so that each spectrum had zero points before the first and after the last band in the spectral range of interest (1500 cm⁻¹ to 1800 cm⁻¹). Peak fitting was performed with OriginPro 2017 software. Firstly, the second derivative of the respective spectrum was calculated to obtain the peak maxima of the spectrum, which are located at the minima of the second derivative. Fitting was done with the “Peak Analyzer” function between 1400 cm⁻¹ and 1750 cm⁻¹ with fixed peak centres at the known positions. The shape of the bands was a Gaussian function.

To calculate the inputs of helical and sheet-like secondary structures, the areas of the fitted bands assigned to secondary structures were used. The inputs for helical and sheet-like structures in % were calculated with the following equations, respectively:

$$I_h = \frac{A_h}{A_h + \sum A_s} \cdot 100$$

$$I_s = \frac{\sum A_s}{A_h + \sum A_s} \cdot 100$$

with the input of helical and sheet-like structures I_h and I_s , respectively, and the area of a fitted band assigned to helical and sheet-like structures A_h and A_s , respectively.

Scanning electron and helium ion microscopy. Scanning electron microscopy images were captured on a Raith e-LiNE microscope and helium ion microscopy (HIM) images on a Zeiss Orion Nanofab microscope. All images were processed with Fiji2 software.

Computational Details

All calculations were performed in a vacuum using the GPAW code based on the projector-augmented wave formalism. The Bayesian error estimation functional with van der Waals correlation¹ was employed together with the grid-based finite-difference basis set. A 5 x 5 graphene super cell was constructed, containing 72 carbon atoms. The dimensions of the super cell were set to 14.82 Å x 14.82 Å x 20.76 Å to exclude interactions between neighboring cells in z-direction. To obtain laser-oxidized graphene, one epoxide and one hydroxyl group were placed on top of the graphene monolayer. The resulting graphene-based surfaces were optimized in to obtain the total energy E_{surface} . The structure of Fmoc-Phe was obtained from PubChem (compound ID 978331) and optimized as a monomer (with the total energy $E_{\text{Fmoc-Phe}}$) before adding it to the surfaces.

Finally, Fmoc-Phe was added on the surfaces. The surface-Fmoc-Phe distance and orientation was varied and the systems were optimized to obtain the total energy E_{system} of the complex. The number of k-points was 4x4x1 to obtain an energy difference of less than 0.05 eV.

The adsorption energy E_{ads} of each system was calculated using the following equation:

$$E_{\text{ads}} = E_{\text{system}} - (E_{\text{surface}} + E_{\text{Fmoc-Phe}})$$

with parameters described above.

S2. Sample optimization

Fmoc-Phe gelled in Phosphate Buffer Saline (PBS) solution, at a concentration of 0.2 w%, following a heating/cooling cycle. Before assessing the gel network on the graphene surfaces, we investigated gelation on mica discs (Table S1) to determine the optimal conditions for sample handling and microscopy imaging (such as Fmoc-Phe concentration, network thickness and drying methods).

For AFM imaging – and s-SNOM as an AFM-based method – a flat background with distinct structural features is a prerequisite for obtaining high-resolution images. Therefore, the desired Fmoc-Phe gel sample should provide distinct, spatially separated fibres on the flat surface. This implies that the concentration of Fmoc-Phe should be low enough to avoid the formation of a rather dense fibrous network. The minimum gelation concentration (MGC) of Fmoc-Phe is 0.2 wt.-%². Below the MGC, the supramolecular network is too weak to form a self-supporting gel. However, the self-assembly process does occur, resulting in a viscous solution with a less dense network. To evaluate fibre density, we prepared Fmoc-Phe xerogel samples (gels dried overnight at rt in open air) at a range of concentrations (0.1 wt.-%, 0.2 wt.-% and 0.3 wt.-%). Optical images (Fig. S1) showed the formation of different densities (crystals) depending on concentration. At 0.1 wt.-% and 0.2 wt.-%, distinct, round-shaped, concentric crystals formed on the mica surface. Nano-FTIR analysis of the crystals showed that they consist of PBS salts (Fig. S2, section S3). Although PBS concentration is constant in all samples, the density of PBS crystals is affected by the Fmoc-Phe concentration. Indeed, the crystal density was lower at 0.1 wt.-% Fmoc-Phe samples than at 0.2 wt.-%. At 0.3 wt.-%, a thick xerogel layer was visible, lacking distinct crystalline structures. It is of note that the formation of crystals or fibres depends on the drying method (*vide infra*). Additionally, fibres could not be observed with optical microscopy. An increased gelator concentration seems to hinder the formation of distinct crystals. Therefore, since we aimed for the least dense gel network, 0.1 wt.-% was chosen as the optimal concentration for sample preparation.

SEM and HIM imaging are performed under vacuum; therefore, a dry sample (xerogel) is required. The drying method of wet gels can significantly impact the supramolecular network.^{3,4} Indeed, during drying, the 3D network collapses to 2D, which appears denser. In practice, no wet and dry gels can be compared. Single fibres tend to aggregate into thicker bundles during drying, which again aggregate to higher-ordered structures than in wet gels.^{4,5} To obtain the most realistic image of the supramolecular fibrous network, the drying time should be as short as possible. For example, freezing at -20 °C for 7 h and subsequent lyophilization leads to a rather realistic result.⁴ For Fmoc-Phe gels, the molecular arrangement of the gelator molecules is retained after lyophilization.² We therefore prepared a xerogel sample on mica by freezing and subsequent lyophilization, while a reference sample was dried under vacuum at rt. The latter showed similar, round-shaped crystals as the samples dried at rt in open air (Table S1 and Fig. S1). The crystals of the freeze-dried/lyophilized sample were elongated in shape and partially aligned in a parallel manner. This observation suggests that round-shaped concentric crystals form due to the slow evaporation of the solvent, which presumably could lead to variations in the morphology and density of the Fmoc-Phe fibres. Therefore, for the analysis of Fmoc-Phe fibres, we have chosen lyophilization as a standard method for sample preparation, as it yields the most realistic image of the surface-gel interface.

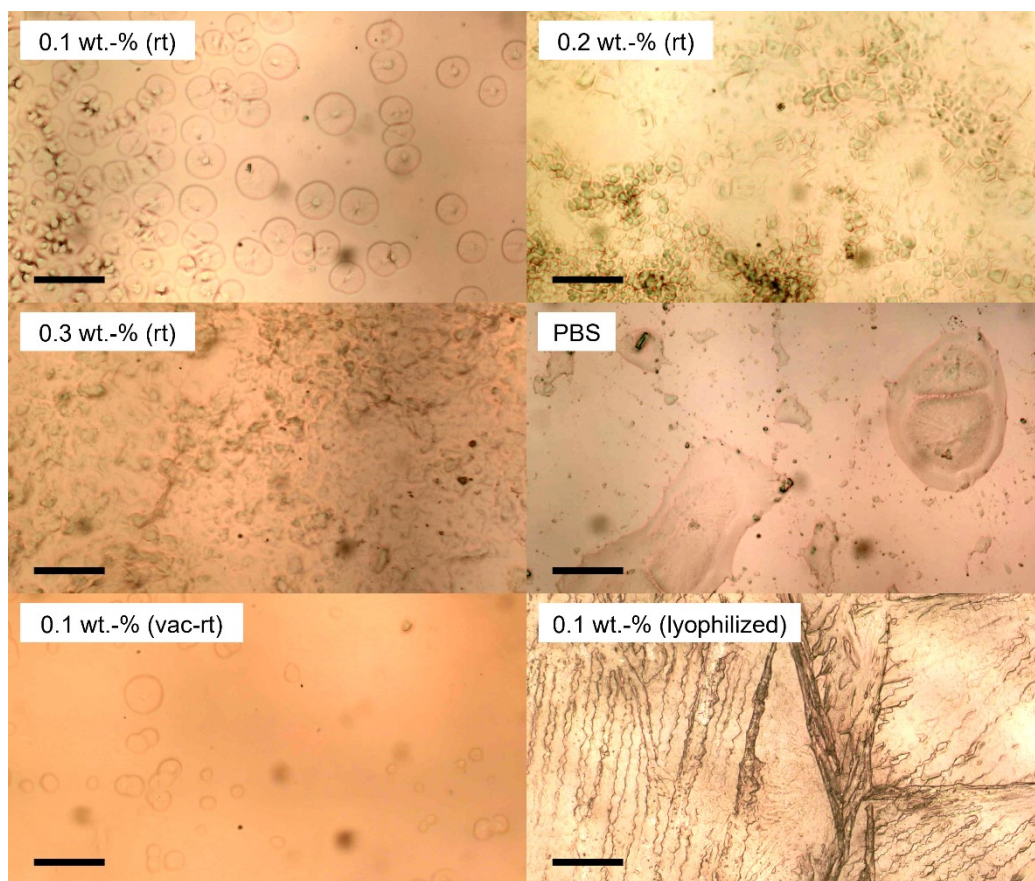


Figure S1: Optical microscopy images of Fmoc-Phe on Mica: rt-dried Fmoc-Phe gel with Fmoc-Phe concentrations of 0.1 wt.-%, 0.2 wt.-% and 0.3 wt.-%, rt-dried PBS solution, vacuumed-rt-dried and lyophilized Fmoc-Phe gel, both with an Fmoc-Phe concentration of 0.1 wt.-%. The black scalebars correspond to 50 μm in all images.

S3. Characterization of concentric crystals

The AFM image (Fig. S2A) of the concentric crystal showed a symmetric nanostructure, while HIM (Fig. S2B) and SEM (Fig. S2C) images revealed gel fibres on top of the crystal. To clarify the composition of the crystals, a control sample was prepared on mica, using a hot PBS solution without any Fmoc-Phe molecules. The sample contained various shapes of crystals. A few centred, round crystals were found, while other shapes dominate (Fig. S1). A nano-FTIR spectrum was measured from one crystal to analyse the chemical identity of the crystals. Figure S2-D shows the nano-FTIR spectrum of the crystal (red), the graphene background (black) and the ATR-FTIR spectrum of the PBS salt used to prepare the buffer (blue). The spectrum of the crystal follows the spectrum of the PBS salt with slight deviations. This indicates that the crystal consists of buffer salts. However, the symmetric shape forms when surrounded by Fmoc-Phe fibres, which indicates that the Fmoc-Phe network affects the shape of the crystals.

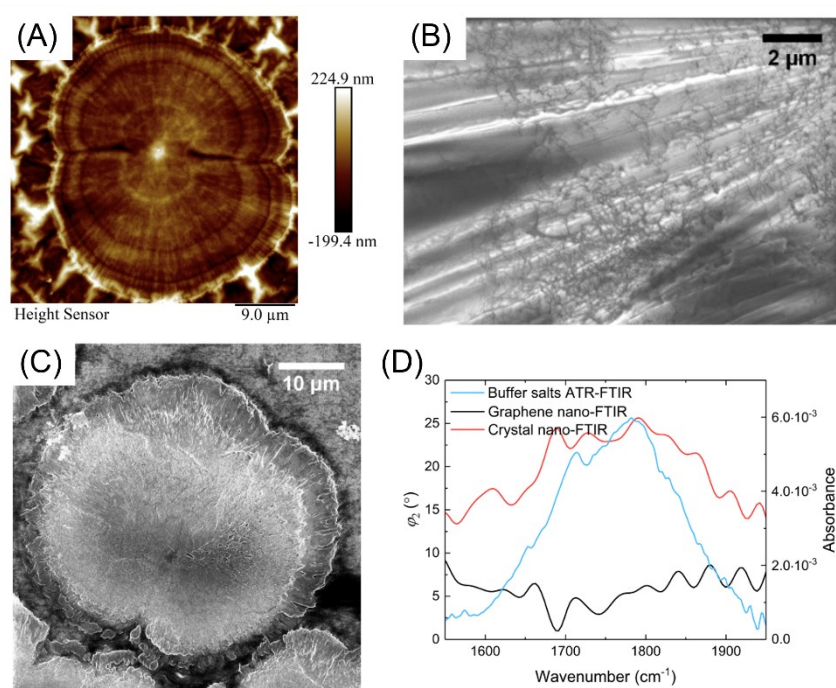


Figure S2: Concentric crystals on rt-dried Fmoc-Phe gel samples on prG: AFM (A), SEM (B), HIM (C) images and nano-FTIR spectra of prG and crystal and ATR-FTIR spectrum of the buffer salts (D).

S4. Raman spectroscopy of pristine and oxidized graphene

After the laser-oxidization of graphene, oxidization was verified by Raman spectroscopy. Figure S3 represents Raman spectra of one pristine and one oxidized area on the same sample. Two bands are observable in both pristine and laser-oxidized graphene: The G band, which is assigned to stretching in the sp^2 carbon lattice of graphene and the 2D band, which is derived from a second-order double-resonant process. The spectrum of laser-oxidized graphene also shows the D and D' bands, which reveal defects in the graphene lattice. The latter is visible as a shoulder of the G band. By adding oxygen-containing functional groups to the graphene surface during laser-oxidization, defects are introduced, which give rise to the D and D' bands.

The Raman spectra were recorded with a DXR Raman (Thermo Scientific), equipped with a 50x objective. The excitation wavelength was 532 nm, and the laser power was 0.5 mW.

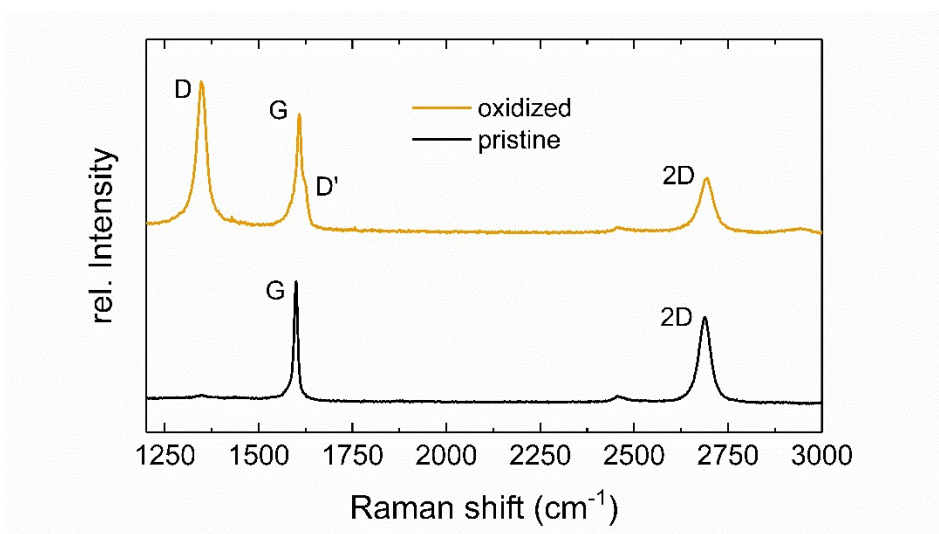


Figure S3: Raman spectra from pristine (black) and laser-oxidized (orange) graphene monolayer.

S5. Nano-FTIR spectra locations and description

The nano-FTIR spectra were taken from five and six different locations on oxidized and pristine graphene, respectively. The exact locations are shown in figure S4 A-D together with the 3rd harmonic phase spectra (Fig. S4 E-F).

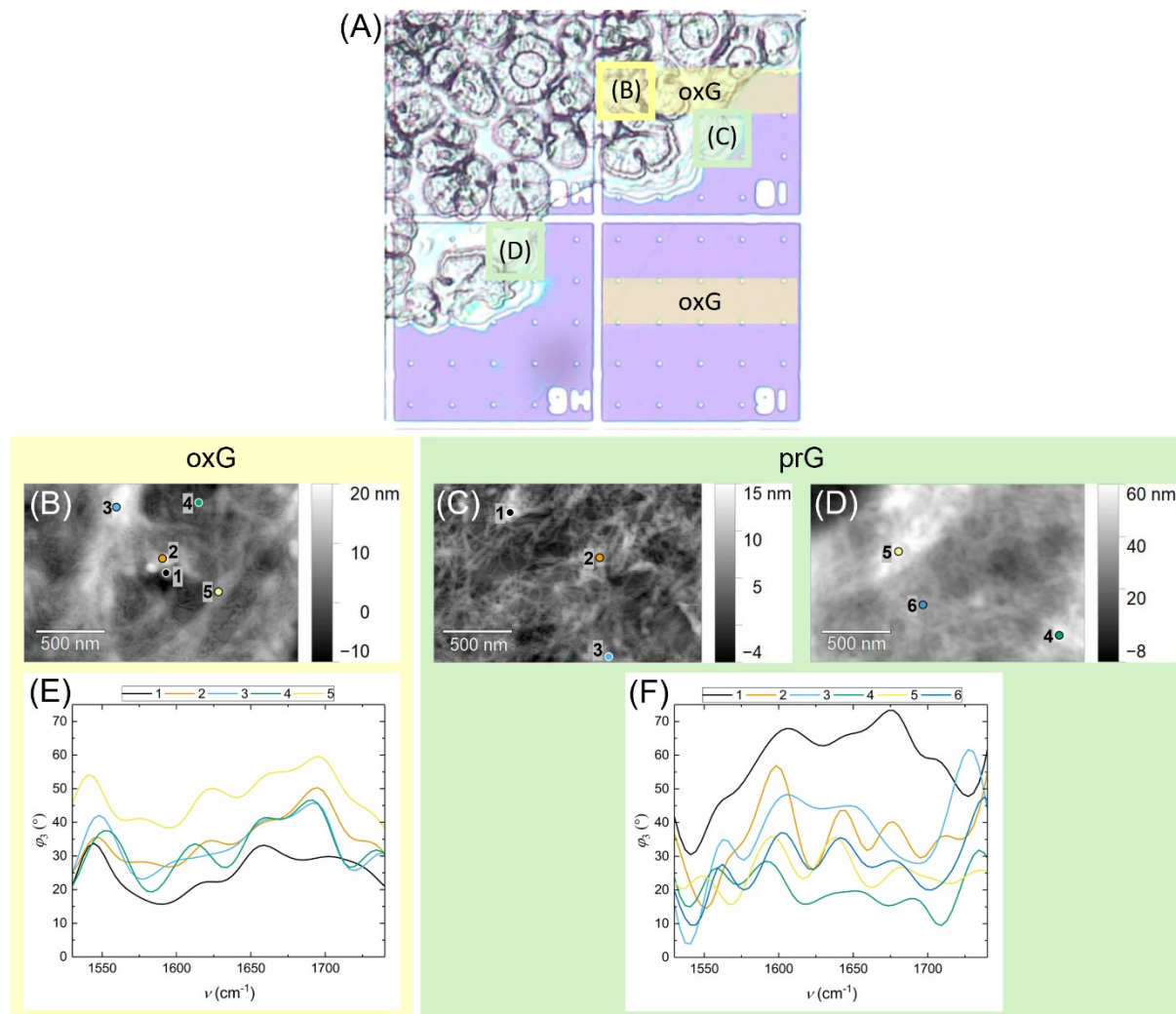


Figure S4: Locations of measured nano-FTIR spectra: (A) Optical microscopy image indicating the oxidized areas and locations of AFM images (B), (C) and (D), which again reveal the exact locations of all nano-FTIR spectra on oxG (E) and prG (F).

S6. Density Functional Theory calculations

In the first step, the pristine and oxidized graphene surfaces, as well as the Fmoc-Phe molecule were optimized in a 14.82 Å x 14.82 Å x 20.76 Å super cell. Figure S5 shows the optimized components. The Fmoc-Phe was added on top of the surfaces in distinct orientations and distances to find the energetically most preferable structures. Table S2 lists all calculated structures, including the adsorption energies of Fmoc-Phe on the surface and the surface-monomer distances.

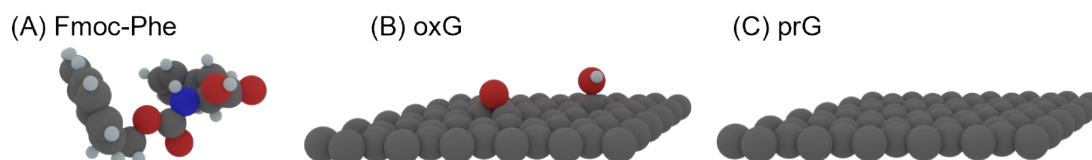
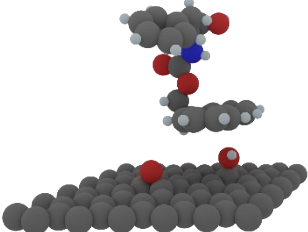
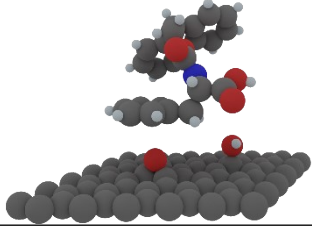
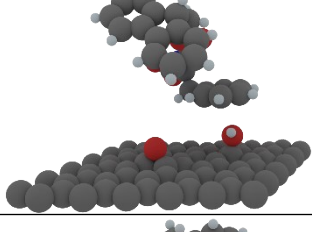
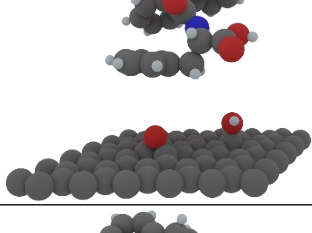
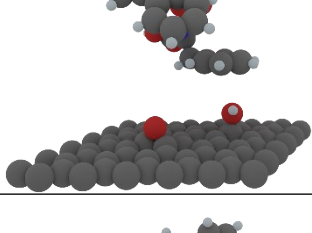
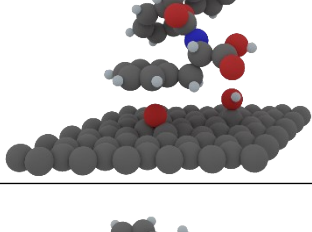
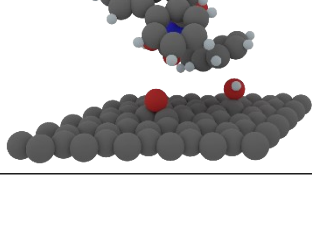
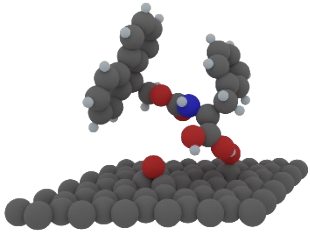
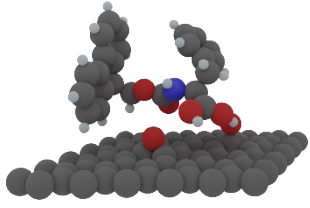
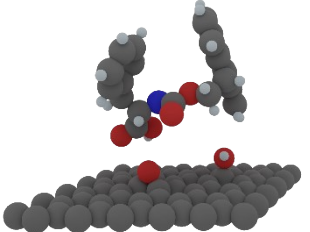
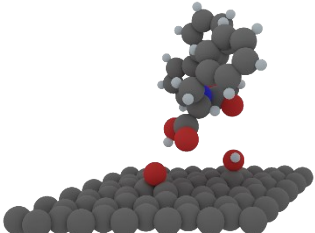
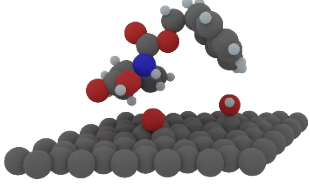
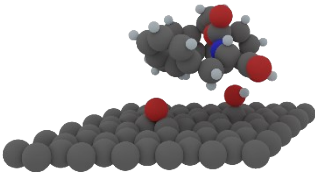
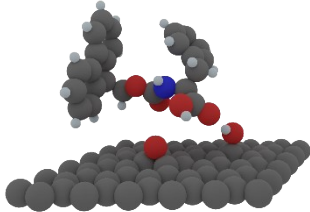


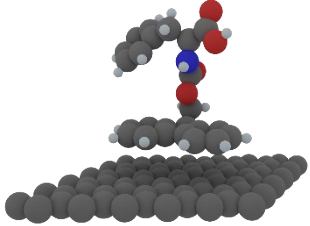
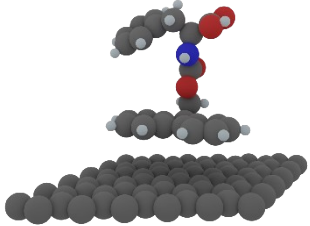
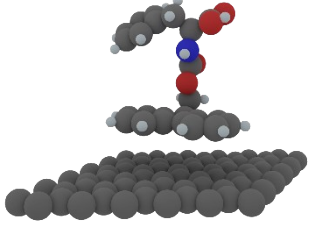
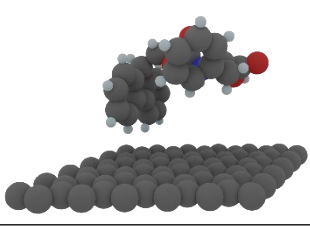
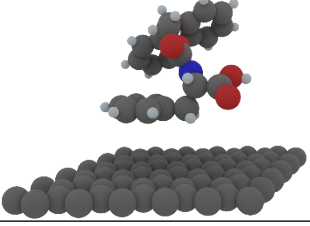
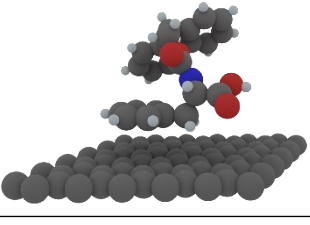
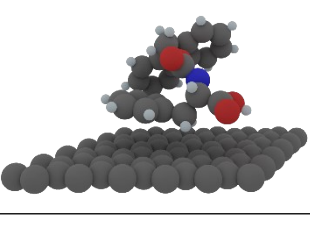
Figure S5: Structures of the optimized components before adsorption energy calculations. The calculated potential energies are (A) -585.11 eV, (B) -1260.04 eV and (C) -1223.25 eV.

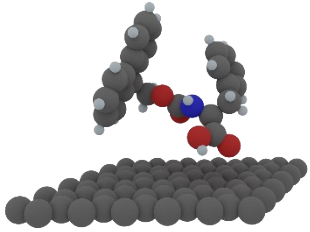
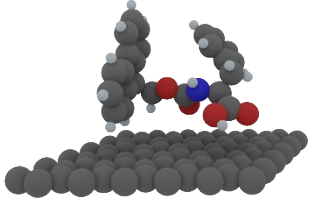
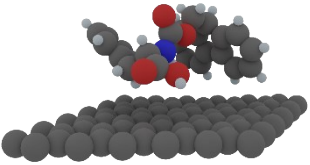
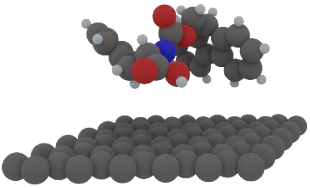
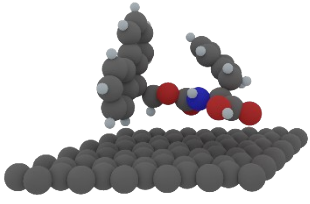
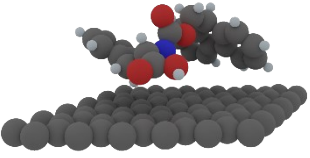
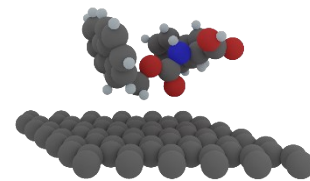
Table S2: List of all optimized structures from the DFT calculations, including surface type, the Fmoc-Phe moiety pointing to the surface, adsorption energy, distance between the surface and Fmoc-Phe (between the two closest atoms) and the optimized structure. Bold text indicates structures discussed in the manuscript.

Surface	Fmoc-Phe moiety pointing to the surface	Adsorption Energy (eV)	Surface-monomer distance (Å)	Structure
oxG	Fluorenyl group (F)	-0.389298	3.199	
oxG	F	-0.257192	2.788	
oxG	F	-0.400973	3.131	
oxG	F	-0.229931	2.912	

Surface	Fmoc-Phe moiety pointing to the surface	Adsorption Energy (eV)	Surface-monomer distance (Å)	Structure
oxG	F	-0.176901	2.901	
oxG	Phenyl ring (P)	-0.200131	3.387	
oxG	P	-0.231245	2.856	
oxG	P	+0.035285	4.928	
oxG	P	-0.079452	3.409	
oxG	P	-0.231245	2.943	
oxG	P	-0.401081	2.884	

Surface	Fmoc-Phe moiety pointing to the surface	Adsorption Energy (eV)	Surface-monomer distance (Å)	Structure
oxG	Carboxylic Acid (COOH)	-0.448214	2.428	
oxG	F/COOH	-0.766519	2.708	
oxG	COOH	-0.225065	3.117	
oxG	COOH	-0.335819	2.261	
oxG	P/Amide N-H	-0.629901	3.028	
oxG	P/COOH	-0.733678	2.903	
oxG	COOH	-0.650409	2.152	

Surface	Fmoc-Phe moiety pointing to the surface	Adsorption Energy (eV)	Surface-monomer distance (Å)	Structure
prG	F	-0.473977	3.649	
prG	F	-0.556214	4.217	
prG	F	-0.629435	3.848	
prG	F	-0.345276	4.900	
prG	P	-0.188953	4.897	
prG	P	-0.508591	3.639	
prG	P	-0.622241	3.489	

Surface	Fmoc-Phe moiety pointing to the surface	Adsorption Energy (eV)	Surface-monomer distance (Å)	Structure
prG	COOH	-0.296705	3.200	
prG	F/COOH	-0.622007	3.472	
prG	F/P/COOH	-0.766176	3.674	
prG	F/P/COOH	-0.248640	4.888	
prG	F/COOH	-0.662321	2.682	
prG	F/P/COOH	-0.892036	3.222	
prG	F/Amide C=O	-0.442086	3.715	

S7. References

1. J. Wellendorff, K.T. Lundgaard, A. Møgelhøj, V. Petzold, D. D. Landis, J. K. Nørskov, T. Bligaard and K. W. Jacobsen, *Phys Rev B*, 2012, **85**, 235149.
2. V. Singh, K. Snigdha, C. Singh, N. Sinha and A. K. Thakur, *Soft Matter*, 2015, **11**, 5353–5364.
3. D. J. Adams, *Gels*, 2018, **4**, 32.
4. L. L. E. Mears, E. R. Draper, A. M. Castilla, H. Su, Zhuola, B. Dietrich, M. C. Nolan, G. N. Smith, J. Douth, S. Rogers, R. Akhtar, H. Cui and D. J. Adams, *Biomacromolecules*, 2017, **18**, 3531–3540.
5. B. Yang, M. Lledos, R. Akhtar, G. Ciccone, L. Jiang, E. Russo, S. Rajput, C. Jin, M. G. F. Angelereou, T. Arnold, J. Rawle, M. Vassalli, M. Marlow, D. J. Adams and M. Zelzer, *Chem Sci*, 2021, **12**, 14260–14269.